

# **Effect of Film Formation Method and Annealing on Morphology and Crystal Structure of Poly(L-Lactic Acid) Films**

Shan-Ting Hsu, Y. Lawrence Yao

Department of Mechanical Engineering, Columbia University, New York, NY, 10027, USA

## **Abstract**

The poly(L-lactic acid) (PLLA) has potential medical usage such as drug delivery since it can degrade into bioabsorbable products in physiological environments, while the degradation is affected by its crystallites. In this paper, the effects of film formation method and annealing on the crystallites formed in PLLA films are investigated. The films are made through solvent casting and spin coating, and subsequent annealing is conducted. The resulting morphology, molecular order, conformation, and intermolecular interaction are examined using optical microscopy, wide-angle X-ray diffraction, and Fourier transform infrared spectroscopy. It is observed that solvent casting produces category 1 spherulites while annealing the spin coated films leads to spherulites of category 2. The crystal structure of the two kinds of films also shows distinct features. The results enable better understanding of the crystallites in PLLA, which is essential for its medical application.

## **1 Introduction**

There is a significant interest in use of biodegradable polymers due to their biocompatibility and biodegradability. Poly lactic acid (PLA) is a biodegradable polymer and can be obtained from renewable sources such as corn starch. It has a wide range of applications in food packaging

and tissue engineering. It is also preferred in drug delivery because it can degrade into bioabsorbable products in physiological environments. Its degradation mainly comes from the cleavage of its ester groups, and is sensitive to chemical hydrolysis. In this application, drug molecules are encapsulated in the polymer by dispersing or dissolving in the polymeric solution, formed through melting the polymer or dissolving it in a solvent. During the process polymer may crystallize, which influences its degradation [1]. Tsuji and Ikada [2] proposed that the degradation of PLA begins in the amorphous region between the lamellae, followed by the disorientation of the lamellae and disappearance of the spherulitic structure. Namely, crystallites affect PLA degradation and thus play a significant role when the material is used in the drug delivery system.

Efforts have been done to investigate the crystallization behavior and resulting crystal structures of PLA films. Among them, solvent casting [3,4] and spin coating [5] are the two commonly used film formation methods. Solvent casting is a simple film formation technique in which quiescent polymer solution is deposited on a substrate, while evaporation of solvent leaves the solid polymer film. This process generally takes hours. During the casting process crystallization could occur in solution if the evaporation rate is low enough for polymer molecules to diffuse to the crystal growth front and overcome the energy barrier of deposition, so that crystals can grow. Category 1 spherulites, in which lamellae grow in all directions and the spherical symmetry extends to the central region as defined by Norton and Keller [6], can be commonly observed in the as cast films [3,7]. Spin coating generates polymer films with thinner and more uniform thickness. It involves rapid rotation of polymer solution, with the centrifugal force pushing it to flow radially outward, decreasing its thickness. The solvent evaporates simultaneously. This process typically finishes within several seconds or minutes.

Due to rapid evaporation, it is less likely for crystallites to develop in the as coated films.

To increase crystallinity in as cast/coated PLA films, further annealing has been attempted. For the as cast films fully covered by spherulites formed during casting, subsequent annealing increases the degree of crystallinity, but does not alter the morphology [3,4]. As coated films are generally amorphous. Annealing such films from the glassy state can generate crystal structures different from those developed in as cast films. One common feature is the nodular structure [8-10]; the nodule is the nanometer-sized crystalline particle developed during annealing from the glassy state [11]. As annealing time and/or temperature increase, the nodules enlarge, and may develop into larger needle-like crystals [8]. It is also observed that nodules develop into lath-like lamellae through merging or lateral aggregation [9,10]. At larger scale, the sheaf-like structures can be observed [12,13], and category 2 spherulites, in which lamellae grow unidirectionally in the central region and the spherical symmetry does not extend to the center [6], are developed [14]. Crystal structures developed by annealing from the glassy state thus show distinct features from those developed in solution.

In spite of the fact that different film formation methods and subsequent annealing lead to different morphologies and crystal structures, their effects have not been fully explored. Pluta and Galeski [15] conducted the wide-angle X-ray diffraction (WAXD) measurement on PLA films crystallized from melt and glass, and peculiarity in the WAXD profiles for the latter is noticed. It reveals further information of the crystal structure, which is not clear. Li et al. [5] observed various PLA film morphologies crystallized from glass, while the crystal structure is not addressed. For annealed solvent cast PLA films, crystal structures developed in the two crystallization steps are expected to be different. The difference has not drawn much attention.

It is also worth considering the causes leading to different morphologies in the films.

The objective of this study is to investigate the morphology and crystal structure in the PLA films formed through solvent casting and spin coating followed by annealing. The morphology is observed by optical microscopy, and crystal structure is studied through the WAXD and Fourier transform infrared (FTIR) measurement. The former is utilized to study the molecular order and the latter is to investigate the conformation of molecules and intermolecular interaction.

## **2 Background**

Poly (L-lactic acid) (PLLA) has a glass transition and melting temperatures of around 60°C and 175°C respectively, and can crystallize in  $\alpha$ ,  $\beta$ , and  $\gamma$  forms depending on crystallization conditions. The  $\alpha$  form exists in solvent cast and annealed samples, and the unit cell structure is orthorhombic with two  $10_3$  polymeric helices [16-18]. The lattice parameters are  $a=10.66 \text{ \AA}$ ,  $b=6.16 \text{ \AA}$ , and  $c=28.88 \text{ \AA}$  [17], but the values may be slightly different [16,18,19]. In the orthorhombic unit cell, PLLA chains are folded in the  $\langle 110 \rangle$  direction [17,20].

### **2.1 Nucleation and crystallization**

Polymer crystallization in dilute solution is composed of induction period, primary crystallization, followed by secondary crystallization. The induction period is the time to obtain steady nuclei before crystallization can occur [21]. In primary crystallization, spherulites are developed and eventually impinge with each other. Crystallization can continue after the impingement, known as the secondary crystallization. It is contributed by the amorphous chains within the lamellae with slower crystallization rates due to chain imperfection [22].

Crystallization from the melt follows a different route, in which nanometer-sized nodules are developed first followed by coalescing with each other to form larger crystals such as lamellae [9]. The concurrent orientation adjustment of neighboring nodules is required for perfect coalescence. This crystallization route accounts for annealing of the as cast/coated film and the resulted crystal structures.

## 2.2 Mobility of polymer molecules in solution and melt

Polymer molecules move via diffusion, and the diffusion coefficient  $D$  is proportional to mobility  $\mu$  via  $D=\mu k_B T$ , with  $k_B$  the Boltzmann constant and  $T$  temperature. The value  $D$  is related to solution concentration, which is divided into dilute, semidilute, and concentrated. Molecules in dilute solutions are separated, occupying a spherical region of radius  $R_g=b\sqrt{N/6}$  where  $b$  and  $N$  are the length and number of submolecules, respectively [23]. As the concentration increases, the polymer coils start to overlap at the concentration  $c^*$  given as [24]

$$\frac{\frac{M}{N_A}}{\frac{4}{3}\pi R_g^3} \leq c^* \leq \frac{\frac{M}{N_A}}{R_g^3} \quad (1)$$

where  $M$  is molecular weight and  $N_A$  is the Avogadro constant. In the concentrated solution, such as the polymer bulk above its glass transition temperature, the concentration fluctuation is negligible. The cross-over concentration from semidilute to concentrated  $c^{**}$  is [23]

$$c^{**} \cong \frac{\nu \frac{M_s}{N_A}}{b^6} \quad (2)$$

where  $\nu$  and  $M_s$  are the excluded volume and molecular weight of the segment, respectively.

For dilute solution, the Stokes-Einstein equation gives the diffusion coefficient

$$D = \frac{k_B T}{6\pi\eta R_H} \quad (3)$$

where  $\eta$  and  $R_H$  are the solvent viscosity and hydrodynamic radius, respectively. The latter is related to the radius of gyration  $R_g$  by  $R_H = 0.537R_g$  [25]. If the concentration is extremely high, the chains are entangled and their movements are described on the basis of the reptation theory [26], and the diffusion coefficient is then given by [23]

$$D = \frac{k_B T}{N\zeta} \quad (4)$$

where  $\zeta$  is a Rouse model parameter.

### 2.3 Structure of spherulites

Spherulites are composed of the crystalline, the amorphous phases, as well as the rigid amorphous phase (RAP). Chains in RAP are immobile and remain vitrified even above the glass transition temperature [27]. In terms of architectures, spherulites can be developed into two categories [6], depending on the competition between the order in the crystal structure and the disorder of the crystallographic orientation; the disorder is associated with the randomization of secondary nucleation at the growth front [28]. The randomness disrupts the crystalline anisotropy. For category 1 spherulites, disrupt occurs early, and multiple directional growth is achieved in the beginning. The disorder disrupts the crystalline anisotropy later for category 2 spherulites, leading to the threadlike structure at the center and sheaf outside.

The origin of disorder during the secondary nucleation is caused by three reasons [28]. The first reason is the static spatial heterogeneity such as foreign particles, which deflect the tip of growing lamellae and perturb their growth directions. The second reason is due to the small rotational diffusion coefficient when compared with translational diffusion coefficient, which

suggests that the molecule has difficulty changing its orientation when depositing on the growth front and thus causes disorder. The third reason is the non-crystallographic branching. From direct AFM observation [29], it may occur at a short distance away from the mother lamellae. This gives evidence that branching is formed by the loose loop or protruding cilia of molecules trapped in the mother lamellae. The third reason dominates based on simulation results [28].

### **3 Materials and Methods**

#### **3.1 Sample preparation and annealing**

PLLA granule samples were provided by PURAC and used as received. The inherent viscosity ( $\eta$ ) in chloroform at 25°C is 1.6 dl/g, and the molecular weight is  $M=56,274$  g/mol from the Mark-Houwink equation,  $\eta=0.454\times 10^{-4}M^{0.73}$  [30]. To prepare solvent cast films, the granules were dissolved in methylene chloride ( $\text{CH}_2\text{Cl}_2$ ) from Sigma Aldrich, with concentration of 0.1 g PLLA/3 mL  $\text{CH}_2\text{Cl}_2$ . The solution is stirred with a magnetic stirrer for 4 hours, and 15 mL solution was cast in a covered Petri dish with a glass slide as a substrate. The solution was left in the hood at 25°C for 24 hours. The film formed on the glass substrate was used as the solvent cast films. Its thickness, measured by profilometry, is 20-25  $\mu\text{m}$ . The solution with doubled concentration was spin-coated on a glass substrate with a rotational acceleration of 255  $\text{rev}/\text{min}^2$  and rotational velocity of 1000 rpm. The film thickness is around 2.5  $\mu\text{m}$ . The thermophysical property and crystallization behavior in films thinner than 1  $\mu\text{m}$  differs from that in thicker films [31]. Since both solvent cast and spin coated films are thicker than 1  $\mu\text{m}$ , the effects of film thickness are insignificant. The films were annealed at 80°C, 110°C, and 140°C for 1 and 3 hours; some spin coated films were annealed at 140°C for 8 and 24 hours. The annealed films were quenched at room temperature after annealing.

### **3.2 Characterization**

Morphology of PLLA films was observed with an optical microscope (Olympus BX60) in the transmission mode. WAXD measurements were accomplished using the Inel X-ray diffractometer. Film specimens were exposed to the monochromatic  $\text{CuK}\alpha$  radiation with wavelength  $\lambda=0.15418$  nm at 40 kV and 30 mA. Care was taken to adjust the incident angle of the X-ray to prevent penetration into the substrate. A Perkin Elmer Spectrum 400 FTIR spectrometer with attenuated total reflectance (ATR) attachment using ZnSe crystal was used to measure the IR spectrum of the films peeled from the glass substrate. The data were recorded with a  $4\text{ cm}^{-1}$  resolution.

## **4 Results and Discussion**

### **4.1 Morphology**

Spherulites already appear and impinge in solvent cast films before annealing because solvent evaporates at a rate low enough for crystals to grow during the casting process. The spherulitic structure resembles category 1, and remains unchanged after annealing. The morphology for the annealed solvent cast film is given in Fig. 1(a). No crystallite exists in spin coated films before annealing as will be confirmed by WAXD. This is due to the fact that during coating, the solvent evaporates faster than the induction period. It is pointed out that for linear poly(decamethylene terephthalate) with molecular weight approximately 40,000 crystallized in solution at  $32.1^\circ\text{C}$ , the induction period is between 6 and 34 minutes for solution concentration between 10 and 2.5% [32]. Because of the similarity of the molecular weight and crystallization temperature, the induction time of the PLLA in this study is expected to be on the order of minutes, which is much longer than the solvent evaporation time (less than 45 seconds,

assuming all the solvent evaporates by the end of coating process). It is reasonable to obtain an amorphous structure through spin coating.

After annealing the spin coated films, paired dots are developed with a bright threadlike fiber in between, which are category 2 spherulites, as shown in Fig. 1(b). The difference between the two categories results from the order of the secondary nucleation: if disorder disrupts the orientation of crystal growth early, category 1 spherulites can be generated, and non-crystallographic branching is a main reason causing the disorder [28]. The different branching behaviors in the two films results from the different amount of supplying chains at crystallization sites. The chains are carried by a compensation flow induced by the volume shrinkage because of crystallization [22], and chain mobility is essential. To investigate the mobility, the concentration and diffusion coefficient are calculated. For the solvent cast films, the spherulites are developed in solution, whose overlap concentration, calculated from Eq. (1), is between 0.6 and 2.3 g/ml. (For calculation, the monomer is taken as the submolecule, and its length is estimated by the size of the unit cell [17]. The number of submolecules is therefore the degree of polymerization,  $56,274/72=782$ .) Since the solution concentration, 0.033 g/ml, is much less than the overlap concentration, the solution is dilute and Eq. (3) is used to determine the diffusion coefficient to be  $3 \times 10^{-6}$  cm<sup>2</sup>/s. Due to extremely high concentration, the molecules in spin coated films experience entanglement during crystallization. Zhang et al. [33] proposed the diffusion coefficients for PLLA bulk above the glass transition temperature as a function of temperature and degree of polymerization. For the temperature around 400 K and the degree of polymerization of 782, the diffusion coefficient is estimated on the order of  $10^{-9}$  cm<sup>2</sup>/s. Their results agree with the relation between diffusion coefficient and chain length stated by Eq. (4). Therefore, during the periods when the spherulites are developed, chain

mobility in the spin coated films is much less than that in the solvent cast films. The scenario of chain movement in the crystallization front in both films can thus be described as follows. For solvent cast films, the high chain mobility enables a flow of surrounding material to the crystallization front to compensate the volume shrinkage, supplying molecules to the branching growth surface, so that branching could easily happen. For spin coated films, due to low mobility, the polymer chains connecting crystalline and non-crystalline regions are entangled with adjacent molecules and hard to relax. The shrinkage is thus not compensated by flow, but by local extension of molecules to the front [22]. Therefore, the supplying material is less available, which is unfavorable to the growth of branches. This explains the origin of different spherulitic structures observed in solvent cast and spin coated films.

For the spin coated films annealed at 140 °C for longer time, the boundaries can be observed more clearly, while the number of observable eye structures is reduced, as shown in Fig. 2. The “disappeared” eyes are essentially enclosed by the lamellae growing in the direction outward from the film, suggesting a later stage of the development of category 2 spherulites. Although the eyes are enclosed, the spherical symmetry does not extend to the center, and the sheaf-like features are preserved, which agrees with the description of category 2 spherulite proposed by Norton and Keller [6] and differentiates from the spherulites formed in the solvent cast films. The existence of the eye structures suggests that lamellae do not branch into the region even in the later stage of development. The possibilities can be twofold. First, the lamellae develop at the expense of the crystallizable material, and the non-crystallizable material, such as atactic components or branched chains, does not participate in crystallization and are accumulated around the growing lamellae. As the lamellae grow and splay, the non-crystallizable material may be trapped in the eyes, which prevents lamellae from branching into it. Another reason

could be the low chain mobility within this region. Some crystallizable chains may be highly entangled and their low mobility makes it hard to relax and crystallize. As such chains accumulate in the eyes, it is more difficult for lamellae to grow into the region.

The morphology of PLLA crystals developed in spin coated films after annealing is a function of film thickness and annealing temperature. Spherulites are observed in the films thicker than 50 nm, annealed at temperatures between 100 and 145 °C, while single crystals and dendrites are formed in a thinner film or at higher annealing temperatures [34]. This agrees with the spherulitic morphology observed in our spin coated films, developed within a 2.5- $\mu\text{m}$  film thickness and annealed at temperatures up to 140 °C. The difference of crystalline morphologies as a function of film thickness can be related to the local chain mobility near the polymer/substrate interface, depending on the interaction between the polymer and substrate. A reduced glass transition temperature has been observed for a PLLA film thinner than 100 nm, suggesting a higher local chain mobility near the surface than in the bulk [35]. Similar results are proposed as stated in Sec. 3.1 [31]. The thickness effect is insignificant in the current study due to the much larger film thickness.

## **4.2 Molecular order**

Chain mobility influences lamellar structures. The lamellae observed in the solvent cast films form in dilute solution, in which chains have high mobility to rearrange into an ordered state and to travel to lamella growth fronts to crystallize. This leads to more uniform lamellae and more regular fold surfaces, as shown in Fig. 3(a). In spin coated films, the lamellae are developed from the melt during the annealing process, and chains entangle with each other experiencing less mobility. Crystallization in the melt thus does not follow the same route as in the dilute

solution, and proceeds in a pathway involving a transient mesomorphic structure [36]. In the beginning, chains close to the lamellae growth front form a mesomorphic structure while they are crystallizing. The crystallizing chains in the mesomorphic structure are ordered while still include conformational defects. The mesomorphic structure thickens with time and with the distance from the lamella growth front. Chain rearrangements occur during the thickening process, and higher ordered crystals are developed eventually. The resulting structure is composed of nanometer-sized nodules in a planar assembly. The nodules coalesce to develop lamellae [9], while fringed micellar crystallization can also occur simultaneously with the folding structure, which roughens the fold surface [37]. The sketch of the lamellar structures in the annealed spin coated film is given in Fig. 3(b).

The WAXD profiles of solvent cast and spin coated films are given in Figs. 4(a) and 4(b). For solvent cast films, the profiles show three stronger peaks, (010), (110)/(200), and (203), while only (110)/(200) and (203) peaks exist for the spin coated films. The (110)/(200) peak remains prominent in all crystalline samples, including the non-annealed solvent cast film with lower degree of crystallinity. (The degree of crystallinity will be discussed below; see Fig. 5.) This suggests the crystal structure in the (110) and/or (200) direction keeps ordered throughout the crystallization process. Since PLLA crystallization begins with chain folding in the  $\langle 110 \rangle$  direction, forming a crystal surface for the subsequent chains to attach [17,20], the (110)/(200) peak may be mainly due to the order of chain folding in the  $\langle 110 \rangle$  direction. The (110)/(200) peak gradually increases with the annealing temperature for solvent cast films, while for spin coated films the peak remains prominent even at lower annealing temperature. This is because the degree of crystallinity of spin coated films is always higher than that of solvent cast films under the same annealing conditions. It is also noted that the (203) peak becomes less

prominent and the (010) peak even disappears for the spin coated films. The observed intensity  $I$  is determined by the polarization factor  $P$ , Lorentz factor  $L$ , multiplicity factor  $j$ , absorption factor  $A$ , and structure factor  $F$ , or  $I = P \cdot L \cdot j \cdot A \cdot |F|^2$  [38]. Since we consider the intensity difference of a single peak in the same material, the first four factors are taken to be the same. The structure factor  $F$  is thus of our interest, and is given as

$$F = \sum_{n=1}^N f_n \exp[2\pi i(hx_n + ky_n + lz_n)] \quad (5)$$

in which  $f$  is the atomic scattering factor accounting for the amplitude of the wave scattered by an atom in a given direction,  $h$ ,  $k$ , and  $l$  are the Miller indices of crystallographic planes, and  $x$ ,  $y$ , and  $z$  are the atomic positions in a unit cell [38]. This equation suggests that the intensity is the summation of the wave amplitude scattered by the  $N$  atoms, and that the atoms need to be located at certain positions for diffraction to occur. The number of atoms is proportional to the area of the reflection plane. This area can be approximated by knowing the sizes of the lateral dimensions of lamellae (on the order of  $\mu\text{m}$ ), the lamellar thickness and the dimensions of the nodules (on the order of  $\text{nm}$ ), and the separation between atomic planes (on the order of  $\text{\AA}$ ). Since the degree of crystallinity is higher in spin coated films, the total area is expected to be larger. This calculation therefore cannot explain the decrease of the (203) peak and disappearance of the (010) peak in spin coated films. The cause is thus given by the atomic positions, or chain packing, which affects the structure factor and thus the observed intensity. Accordingly, in spin coated films, although chains fold orderly, generating strong (110) peak, their packing is less orderly, diminishing the two peaks related to chain packing, (010) and (203). If the spin coated films are annealed longer (8 and 24 hours), the (010) peak begins to emerge, as given in Fig. 4(b) for 24-hour annealing. This shows that longer annealing time favors better

packing of the folded chains and more ordered reflection planes.

The intensity ratio of the two strongest peaks, (110)/(200) and (203), is calculated based on the area under the peaks. The results for 3-hour annealed films are given in Fig. 5, while the results for 1-hour annealing are similar. The ratio for the spin coated films is always higher because of the smaller (203) peaks as discussed above. This ratio does not change with annealing temperature, which suggests that similar crystal structures are formed at the three annealing temperatures. For solvent cast films, the ratio gradually increases with annealing temperature. This higher ratio could come from the newly formed crystallites, since the degree of crystallinity increases with annealing temperature. This increase is because the newly formed crystallites do not develop in solution, but in an environment similar to the spin coated films. From the above discussion, the chains may not pack well and have a smaller (203) peak.

Figure 6 shows the location of the (110)/(200) peak for 3-hour annealed films. Similar trend is observed for 1-hour annealing. Similar trend is observed for 1-hour annealing. The peak location for the spin coated films is smaller than that for solvent cast films. From the Bragg's law, spin coated films have larger d-spacings and thus less ordered and compact crystal structure, which agrees with the discussion above. This can originate from the effect of folds [19]: irregular fold surfaces prevent ordered chain packing, increasing the basal area ( $a$  and  $b$ ) of the unit cell, while  $c$  remains unchanged. As discussed, the lamellar fold surface in the spin coated films is rougher, which leads to larger  $a$  and  $b$ . Based on the plane spacing equation for orthorhombic cells

$$\frac{1}{d^2} = \frac{h^2}{a^2} + \frac{k^2}{b^2} + \frac{l^2}{c^2} \quad (6)$$

where  $d$  is the d-spacing value, larger  $a$  and  $b$  result in larger  $d$ , and therefore smaller  $2\theta$  values.

Higher annealing temperature gives energy to the molecules to achieve equilibrium state, and also enables them to change their conformations to favor chain packing. This explains the smaller d-spacing in the 140°C-annealed spin coated film. We do not observe the change of  $2\theta$  values in solvent cast films with annealing temperature. This is because the dominant spherulitic structure is formed during the same casting process, and the effect of annealing is less significant. The  $2\theta$  values differ in solvent cast films and spin coated films, and the calculated value based on the lattice parameters proposed by Miyata [17] is 16.82°. The values vary slightly due to different processing and crystallization conditions as discussed, which demonstrates that the lattice parameters of polymers can vary even for the same material.

The WAXD profiles in Fig. 4 are composed of amorphous diffraction and crystal diffraction. The dotted line, obtained from amorphous PLLA, is the amorphous diffraction. The integrated intensity of the amorphous diffraction,  $I_a$ , is the area under the amorphous diffraction curve, while the integrated intensity of crystal diffraction,  $I_c$ , is the peak area. Crystallinity is the ratio of  $I_c$  to  $I_a+I_c$  and can be calculated accordingly [39] with results given in Fig. 7. The degree of crystallinity increases with annealing temperature, as expected. Similar results are obtained for the 1-hour annealed films, except that the degree of crystallinity of the 1-hour annealed spin coated films is slightly less than that of the 3-hour annealed spin coated films by 3%. The degree of crystallinity for 1-hour and 3-hour annealed solvent cast films are the same, and 1 hour is found to be long enough to complete the secondary crystallization in solvent cast films. It is also noticed that the degree of crystallinity for the solvent cast films is always lower than the spin coated films, which suggests part of amorphous molecules in the solvent cast films cannot crystallize. This could be related to the structure in spherulites. Optical microscopy reveals that the non-annealed solvent cast film is already filled with spherulites, but its degree of

crystallinity is only 26%; the rest 74% is composed of the amorphous chains. Some of them are inherently non-crystallizable due to branching or atactic configuration, while some are crystallizable. Part of the crystallizable chains may be trapped by the existing lamellar fold surfaces, forming the RAP. The fraction of RAP in crystalline PLLA can be as large as around 20-30% [40,41], which inhibits the development of crystal structure between the lamellae. For spin coated films, no RAP exists in the beginning of the crystallite development, and chains can get crystallized before being trapped by the formed lamellae, leading to a higher degree of crystallinity.

Figures 2 and 4(b) give the crystal information of the spin coated film annealed for a longer time (24 hours), and its degree of crystallinity and peak location are given as a function of annealing time, as given in Fig. 8 which shows that both parameters increase with annealing time. The increase of degree of crystallinity is expected, while the increase of  $2\theta$  value suggests that the crystal structure is more compact and ordered. This figure also shows that the increasing trends tend to level off, which suggests that the crystal structure in the 24-hour annealed film is close to a stable structure and less likely to have further change for even longer annealing time.

#### **4.3 Conformation of molecules and intermolecular interaction**

The conformation of molecules and intermolecular interaction are studied through FTIR. The spectra of the solvent cast and spin coated films are given in Figs. 9(a) and 9(b), respectively. The carbonyl (C=O) stretching region, CH<sub>3</sub> and CH bending region, and the skeletal (C-O-C) stretching region show prominent peaks. It is also observed that there is no absorption band at 921 cm<sup>-1</sup> for the amorphous film (the as coated film), while this peak emerges as the material crystallizes. This peak is attributed to the coupling of the CH<sub>3</sub> rocking vibration with the C-C

backbone stretching, and is the characteristic of PLLA  $\alpha$  crystals [42].

Along the molecular chain, there are three skeletal bonds: C-O (ester), O-C $_{\alpha}$ , and C $_{\alpha}$ -C, in which the ester bond can be assumed *trans* [43]. The O-C $_{\alpha}$  bond has two minimal energies when its bond rotation angle  $\phi$  is  $-160^{\circ}$  and  $-73^{\circ}$ , while the C $_{\alpha}$ -C bond has two minimal energies when its bond rotation angle  $\psi$  is  $160^{\circ}$  and  $-48^{\circ}$ . The rotation angles  $\phi=-160^{\circ}$  and  $\psi=160^{\circ}$  are assigned as *trans* (*t*), while  $\phi=-48^{\circ}$  and  $\psi=-73^{\circ}$  are assigned as *gauche* (*g*). Accordingly, there are four conformers leading to four energy minima: *tt*, *tg*, *gt*, and *gg*, which correspond to  $2_1$ ,  $5_1$ ,  $10_3$ , and  $4_1$  helices [44]. The *gt* conformer has the lowest energy and constitutes the crystal structure. Because of the four conformers, the C=O stretching region can be split into four peaks due to intramolecular and intermolecular interactions, and the four peaks are located at  $1776\text{ cm}^{-1}$ ,  $1767\text{ cm}^{-1}$ ,  $1759\text{ cm}^{-1}$ , and  $1749\text{ cm}^{-1}$ , corresponding to the *gg*, *tg*, *gt*, and *tt* conformers, respectively [43]. The spectra of this region of solvent cast and spin coated films are given in Figs. 10(a), 10(b), and 11. For the solvent cast films, annealing makes more prominent band splitting. (The peak resolving will be discussed below.) However, band splitting cannot be visually observed for spin coated films.

To investigate the components in the spectra, their second derivatives are illustrated in Fig. 12. For solvent cast films, two prominent peaks can be seen at  $1757\text{ cm}^{-1}$  and  $1747\text{ cm}^{-1}$ , while two inconspicuous peaks are at  $1777\text{ cm}^{-1}$  and  $1766\text{ cm}^{-1}$ . These four peaks represent the *gt*, *tt*, *gg*, and *tg* conformers, respectively. The most prominent two peaks, *gt* and *tt* are resolved, as given in Figs. 10(a) and 10(b). The intensity ratio of *gt/tt* increases as the film is annealed, which confirms that the crystal structure is preferred by the *gt* conformer. The peak width (defined as the full width at half maximum) of the resolved peaks is shown in Fig. 13. It is observed that,

as the films are annealed, the width of the *gt* peaks decreases, while that of the *tt* peaks almost does not alter. The peak width in FTIR spectrum is related to the homogeneity in the structure: more chemical environments lead to more complicated intermolecular interactions and broadens the peaks, while fewer chemical environments narrow the peaks [45]. Since the *gt* peak is responsible for crystal structure, the narrowing *gt* peaks is because the crystal structure becomes more ordered as the structure gets crystallized, which leads to a more uniform and homogeneous chemical environment. The band width of the *tt* conformer does not change significantly, because the *tt* conformers do not contribute to crystallization, and remain amorphous after annealing.

It is observed that there are two shoulders appearing at  $1754\text{ cm}^{-1}$  and  $1742\text{ cm}^{-1}$  in the derivative spectrum for the non-annealed solvent cast film (Fig. 12). The two shoulders cannot be attributed to any of the four conformers, and represent two peaks splitting from the *gt* and *tt* peaks. They both split toward the lower wavenumbers. Stress in the film is therefore a possible cause, in that it increases the length of a covalent bond, which decreases the bond's atomic force constant, and thus decreases the infrared absorption frequency of bonds for their stretching vibrations. Band shift has been observed to occur at stresses on the order of MPa [46]. For solvent cast films, the stress can be generated during the casting process: as the solvent evaporates, the volume shrinks but the area is constrained by adhesion to the substrate. This constraint creates an internal stress in the films, which is also on the order of several MPa [47]. This solidification process can thus account for the stress which stretches the bonds and thus the observed shoulders in the spectra. After annealing, the  $1754\text{ cm}^{-1}$  shoulder disappears, and the one at  $1742\text{ cm}^{-1}$  also becomes less prominent, because annealing eliminates the internal stress.

For the spin coated films, the two prominent peaks are *gt* and *tt*, located at  $1759\text{ cm}^{-1}$  and  $1746\text{ cm}^{-1}$ , respectively. There are two additional peaks shown at  $1753\text{ cm}^{-1}$  and  $1742\text{ cm}^{-1}$ , which are also located on the right to the *gt* and *tt* peaks, respectively; therefore, internal stress could be the reason of the splitting. In addition to solidification, the centrifugal force during the spinning process is another source of the internal stress [48]. However, this stress is only on the order of only several Pa [49], much less than the stress required to split the band and is less likely to be the reason. The stress induced by solidification is a more reasonable cause. As the film is annealed, the peaks tend to become less prominent, suggesting the decrease of stress. It can also be seen that, in the derivative spectrum for the as coated film, the *tt* peak is much more prominent than the *gt* peak, which is consistent with the fact that this film is amorphous, and may also explain why the band is located at a lower wavenumber in the original spectrum, as seen in Fig. 11.

## 5 Conclusions

It has been shown that both film formation method and annealing have significant influences on morphology and crystal structure of PLLA films. In solvent cast films, category 1 spherulites are developed in solution during the casting process, and further annealing increases the degree of crystallinity without affecting the morphology. Spin coating leads to amorphous structure, and subsequent annealing generates category 2 spherulites. Molecular order in the two kinds of films is also different as investigated via WAXD measurements. The crystal structure is more compact in solvent cast films than in spin coated films, while the lamellae in solvent cast films formed during casting may be unfavorable to further crystallization. The FTIR measurements demonstrate the conformation of molecules and intermolecular interaction in the crystallites, and

also show possible stress in the films. Longer annealing time does not change the spherulitic structure, which confirms that the crystal structure is mainly determined by film formation method and the mobility of polymer chains at which annealing is conducted.

### **Acknowledgement**

Financial support from NSF under CMMI-1030536 is acknowledged. WAXD measurement was carried out at MRSEC, Columbia University. Thanks are also due to Mr. Gen Satoh and Mr. Huade Tan of Columbia University for helpful discussion and editorial assistance.

## References

- [1] Nampoothiri, K. M., Nair, N. R., and John, R. P., 2010, "An Overview of the Recent Developments in Polylactide (PLA) Research," *Bioresource Technology*, **101**, pp. 8493-8501.
- [2] Tsuji, H., and Ikada, Y., 1998, "Properties and Morphology of Poly(L-Lactide). II. Hydrolysis in Alkaline Solution," *J. Polym. Sci. A: Polym. Chem.*, **36**, pp. 59-66.
- [3] Tsuji, H., and Ikada, Y., 1995, "Properties and Morphology of poly(L-Lactide). 1. Annealing Condition Effects on Properties and Morphologies of Poly(L-Lactide)," *Polymer*, **36**(14), pp. 2709-2716.
- [4] Bhatla, A., and Yao, Y. L., 2009, "Effect of Laser Surface Modification on the Crystallinity of Poly(L-Lactic Acid)," *J. Manufacturing Science and Engineering*, **131**, pp. 051004-1-051004-11.
- [5] Li, H., Nie, W., Deng, C., Chen, X., and Ji, X., 2009, "Crystalline Morphology of Poly(L-Lactic Acid) Thin Films," *Eur. Polym. J.*, **45**, pp. 123-130.
- [6] Norton, D. R., and Keller, A., 1985, "The Spherulitic and Lamellar Morphology of Melt-Crystallized Isotactic Polypropylene," *Polymer*, **26**, pp. 704-716.
- [7] Takeda, H., Nakashima, C., and Nasu, N., 2005, "Studies on Structure of Poly( $\epsilon$ -L-Lysine) Spherulite Grown from Solution," *Sen'I Gakkaishi*, **61**, pp. 61-66.
- [8] Zhao, J., Qiu, J., Niu, Y., and Wang, Z., 2009, "Evolutions of Morphology and Crystalline Ordering Upon Annealing of Quenched Isotactic Polypropylene," *J. Polym. Sci. B*, **47**, pp. 1703-1712.
- [9] Su, C. H., Jeng, U., Chen, S. H., Lin, S. J., Wu, W. R., Chuang, W.-T., Tsai, J. C., and Su, A. C., 2009, "Nanograin Evolution in Cold Crystallization of Syndiotactic Polystyrene as Illustrated via In-Situ Small/Wide Angle X-Ray Scattering and Differential Scanning Calorimetry,"

Macromolecules, **42**, pp. 6656-6664.

[10] Hsu, C. C., Geil, P. H., Miyaji, H., and Asai, K., 1986, "Structure and Properties of Polypropylene Crystallized from the Glassy State," *J. Polym. Sci. B*, **24**, pp. 2379-2401.

[11] Ogawa, T., Miyaji, H., and Asai, K., 1985, "Nodule Structure of Polypropylene," *J. Phys. Soc. Japan*, **54**(10), pp. 3668-3670.

[12] Bassett, D. C., Olley, R. H., and Al Raheil, I. A. M., 1988, "On Crystallization Phenomena in PEEK," *Polymer*, **29**, pp. 1745-1754.

[13] Gao, X., Hou, W., Zhou, J., Li, L., and Zhao, L., 2004, "Relationships Between the Crystal Structures and the Multiple Melting Behaviors of Poly(Ethylene 2,6-Naphthalate)," *Macrom. Mater. and Engr.* **289**, pp. 174-180.

[14] Ivanov, D. A., and Jonas, A. M., 1998, "Isothermal Growth and Reorganization upon Heating of a Single Poly(Aryl-Ether-Ether-Ketone) (PEEK) Spherulite, as Imaged by Atomic Force Microscopy," *Macromolecules*, **31**, pp. 4546-4550.

[15] Pluta, M., and Galeski, A., 2002, "Crystalline and Supermolecular Structure of Polylactide in Relation to the Crystallization Method," *J. Appl. Polym. Sci.*, **86**, pp. 1386-1395.

[16] Kobayashi, J., Asahi, T., Ichiki, M., Oikawa, A., Suzuki, H., Watanabe, T., Fukada, E., and Shikinami, Y., 1995, "Structural and Optical Properties of Poly Lactic Acids," *J. Appl. Phys.* **77**(7), pp. 2957-2973.

[17] Miyata, T., and Masuko, T., 1997, "Morphology of Poly(L-Lactide) Solution-Grown Crystals," *Polymer*, **38**(16), pp. 4003-4009.

[18] Sasaki, S., and Asakura, T., 2003, "Helix Distortion and Crystal Structure of the  $\alpha$ -Form of Poly(L-Lactide)," *Macromolecule*, **36**, pp. 8385-8390.

[19] Davis, G. T., Eby, R. K., and Martin, G. M., 1968, "Variations of the Unit-Cell Dimensions

of Polyethylene: Effect of Crystallization Conditions, Annealing, and Deformation,” *J. Appl. Phys.*, **39**(11), pp. 4973-4981.

[20] Kikkawa, Y., Abe, H., Iwata, T., Inoue, Y., and Doi, Y., 2002, “Crystallization, Stability, and Enzymatic Degradation of Poly(L-Lactide) Thin Film,” *Biomacromolecules*, **3**(2), pp. 350-356.

[21] Imai, M., Mori, K., Mizukami, T., Kaji, K., and Kanaya, T., 1992, “Structural Formation of Poly (Ethylene Terephthalate) during the Induction Period of Crystallization: 1. Ordered Structure Appearing before Crystal Nucleation,” *Polymer*, **33**(21), pp. 4451-4456.

[22] Schultz, J. M., 2001, *Polymer Crystallization: The Development of Crystalline Order in Thermoplastic Polymers*, Oxford University Press, New York, Chaps. 4 and 10.

[23] Doi, M., and Edwards, S. F., 1988, *The Theory of Polymer Dynamics*, Oxford University Press, New York, Chaps. 2 and 5.

[24] Cotton, J. P., Nierlich, M., Boue, F., Daoud, M., Farnoux, B., Jannink, G., Duplessix, R., and Picot, C., 1976, “Experimental Determination of the Temperature-Concentration Diagram of Flexible Polymer Solutions by Neutron Scattering,” *J. Chem. Phys.*, **65**(3), pp. 1101-1108.

[25] Akcasu, A. Z., and Han, C. C., 1979, “Molecular Weight and Temperature Dependence of Polymer Dimensions in Solution,” *Macromolecules*, **12**(2), pp. 276-280.

[26] De Gennes, P. G., 1971, “Reptation of a Polymer Chain in the Presence of Fixed Obstacles,” *J. Chem. Phys.*, **55**(2), pp. 572-579.

[27] Menczel, J., and Wunderlich, B., 1981, “Heat Capacity Hysteresis of Semicrystalline Macromolecular Glasses,” *J. Polym. Sci.: Polym. Lett. Ed.*, **19**, pp. 261-264.

[28] Granasy, L., Pusztai, T., Tegze, G., Warren, J. A., and Douglas, J. F., 2005, “Growth and Form of Spherulites,” *Phys. Rev. E*, **72**, pp. 011605-1-011605-15.

- [29] Li, L., Chan, C.-M., Yeung, K. L., Li, J.-X., Ng, K.-M., and Lei, Y., 2001, "Direct Observation of Growth of Lamellae and Spherulites of a Semicrystalline Polymer by AFM," *Macromolecules*, **34**, pp. 316-325.
- [30] Schindler, A., and Harper, D., 1979, "Polylactide. II. Viscosity-Molecular Weight Relationships and Unperturbed Chain Dimensions," *J. Polym. Sci.: Polym. Chem. Ed.*, **17**, pp. 2593-2599.
- [31] Frank, C. W., Rao, V., Despotopoulou, M. M., Pease, R. F. W., Hinsberg, W. D., Miller, R. D., and Rabolt, J. F., 1996, "Structure in Thin and Ultrathin Spin-Cast Polymer Films," *Science*, **273**, pp. 912-915.
- [32] Lanceley, H. A., and Sharples, A., 1966, "A Kinetic Study of Polymer Crystallization from Solution," *Die Makromolekulare Chemie*, **94**, pp. 30-41.
- [33] Zhang, J., Liang, Y., Yan, J., and Lou, J., 2007, "Study of the Molecular Weight Dependence of Glass Transition Temperature for Amorphous Poly(L-Lactide) by Molecular Dynamics Simulation," *Polymer*, **48**, pp. 4900-4905.
- [34] Maillard, D., and Prud'homme, R. E., 2008, "The Crystallization of Ultrathin Films of Polylactides-Morphologies and Transitions," *Can. J. Chem.*, **86**, pp. 556-563.
- [35] Narladkar, A., Balnois, E., Vignaud, G., and Grohens, Y., 2008, "Difference in Glass Transition Behavior Between Semi Crystalline and Amorphous Poly(lactic acid) Thin Films," *Macromol. Symp.*, **273**, pp. 146-152.
- [36] Strobl, G., 2000, "From the Melt via Mesomorphic and Granular Crystalline Layers to Lamellar Crystallites: A Major Route Followed in Polymer Crystallization?" *Eur. Phys. J. E* **3**, pp. 165-183.
- [37] Wunderlich, B., 1976, *Macromolecular Physics*, Academic Press, New York, Vol. 2, Chap.

5.

[38] Alexander, L. E., 1969, *X-Ray Diffraction Methods in Polymer Science*, John Wiley & Sons, New York, Chap. 1.

[39] Campbell, D., Pethrick, R. A., and White, J. R., 2000, *Polymer Characterization*, 2nd ed., Stanley Thornes, Cheltenham.

[40] Wang, Y., Funari, S. S., and Mano, J. F., 2006, "Influence of Semicrystalline Morphology on the Glass Transition of Poly(L-Lactic Acid)," *Macromol. Chem. Phys.*, **207**, pp. 1262-1271.

[41] Sarasua, J.-R., Zuza, E., Imaz, N., and Meaurio, E., 2008, "Crystallinity and Crystalline Confinement of the Amorphous Phase in Polylactides," *Macromol. Symp.*, **272**, pp. 81-86.

[42] Kister, G., Cassanas, G., and Vert, M., 1998, "Effects of Morphology, Conformation and Configuration on the IR and Raman Spectra of Various Poly(Lactic Acid)s," *Polymer*, **39**(2), pp. 267-273.

[43] Meaurio, E., Zuza, E., Lopez-Rodriguez, N., and Sarasua, J. R., 2006, "Conformational Behavior of Poly(L-Lactide) Studied by Infrared Spectroscopy," *J. Phys. Chem.*, **110**, pp. 5790-5800.

[44] Kang, S., Hsu, S. L., Stidham, H. D., Smith, P. B., Leugers, M. A., and Yang, X., 2001, "A Spectroscopic Analysis of Poly(Lactic Acid) Structure," *Macromolecules*, **34**, pp. 4542-4548.

[45] Smith, B., 1999, *Infrared Spectral Interpretation: A Systematic Approach*, CRC Press, Boca Raton, FL, Chap. 1.

[46] Roylance, D. K., and DeVries, K. L., 1971, "Determination of Atomic Stress Distribution in Oriented Polypropylene by Infrared Spectroscopy," *Polym. Lett.*, **9**, pp. 443-447.

[47] Croll, S. G., 1979, "The Origin of Residual Internal Stress in Solvent-Cast Thermoplastic Coatings," *J. Appl. Polym. Sci.*, **23**, pp. 847-858.

[48] Vorotilov, K., Petrovsky, V., and Vasiljev, V., 1995, "Spin Coating Process of Sol-Gel Silicate Films Deposition: Effect of Spin Speed and Processing Temperature," *J. Sol-Gel Sci. and Tech.*, **5**, pp. 173-183.

[49] Chang, C.-C., Wei, K.-H., and Chen, W.-C., 2003, "Spin-Coating of Polyimide-Silica Hybrid Optical Thin Films," *J. Electrochem. Soc.*, **150**(8), pp. F147-F150.

## Figure list

Fig. 1(a) The morphology of solvent cast film annealed at 140°C for 3 hours. The morphology is similar to that of the as cast film.

Fig. 1(b) The morphology of spin coated film annealed at 140°C for 3 hours. The eye structure is observed.

Fig. 2 The morphology of spin coated film annealed at 140°C for 24 hours. Eye structure remains observable while the boundary of spherulites can be more clearly observed. The spherical symmetry does not extend to the center, and the sheaf-like features are preserved.

Fig. 3(a) Sketch of the lamellar structure in solvent cast films.

Fig. 3(b) Sketch of the lamellar structure in spin coated films.

Fig. 4(a) WAXD profiles for solvent cast films annealed at different temperatures for 3 hours. Dotted line under the as cast film is the fitted curve for the amorphous region.

Fig. 4(b) WAXD profiles for spin coated films annealed at different temperatures for 3 hours. Dotted line under the 80°C annealed film is the fitted curve for the amorphous region.

Fig. 5 Intensity ratio  $I_{(110)/(200)}/I_{(203)}$  of the solvent cast and spin coated films annealed for 3 hours. The error bar represents the standard deviation.

Fig. 6 Location of the (110)/(200) peak for the solvent cast and spin coated films annealed for 3 hours. The error bar represents the standard deviation.

Fig. 7 Degree of crystallinity of the solvent cast and spin coated films annealed for 3 hours. Annealing temperature of 25°C means the as cast film. The error bar represents the standard deviation.

Fig. 8 Degree of crystallinity and peak location of the spin coated films annealed at 140 °C for 1, 3, 8, and 24 hours.

Fig. 9(a) FTIR spectra of the solvent cast films before annealing and after annealed in different conditions.

Fig. 9(b) FTIR spectra of the spin coated films before annealing and after annealed in different conditions.

Fig. 10(a) Curve fitting for the *gt* and *tt* conformers in the carbonyl C=O stretching region of the as cast solvent cast film.

Fig. 10(b) Curve fitting for the *gt* and *tt* conformers in the carbonyl C=O stretching region of the solvent cast film annealed at 140°C for 3 hours.

Fig. 11 Carbonyl C=O stretching region of the spin coated films annealed at different temperatures for 3 hours.

Fig. 12 Second derivative spectra of the C=O stretching region for solvent cast and spin coated films before annealing and annealed at different temperatures for 3 hours.

Fig. 13 Peak width of the resolved spectra for the *gt* and *tt* conformers of solvent cast films before annealing and after annealed in different conditions. The error bar represents the standard deviation of the five measurements.

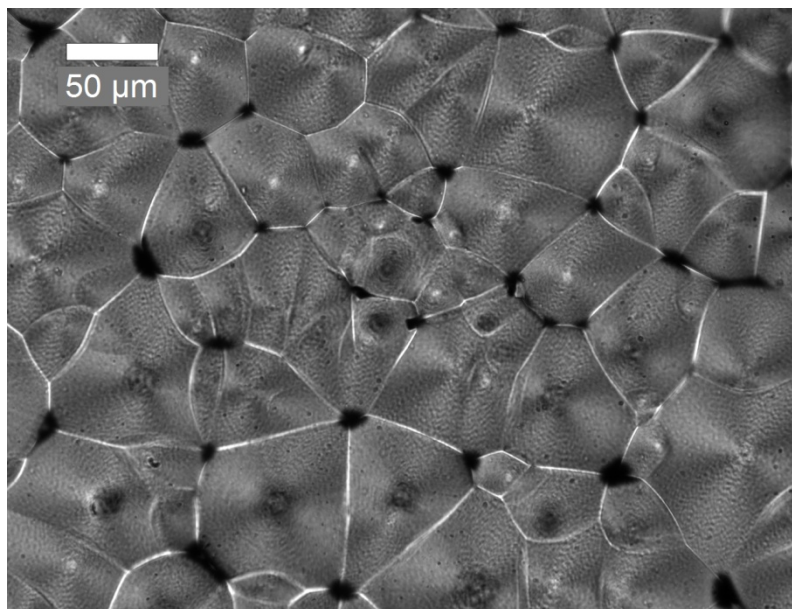


Fig. 1(a) The morphology of solvent cast film annealed at 140°C for 3 hours. The morphology is similar to that of the as cast film.

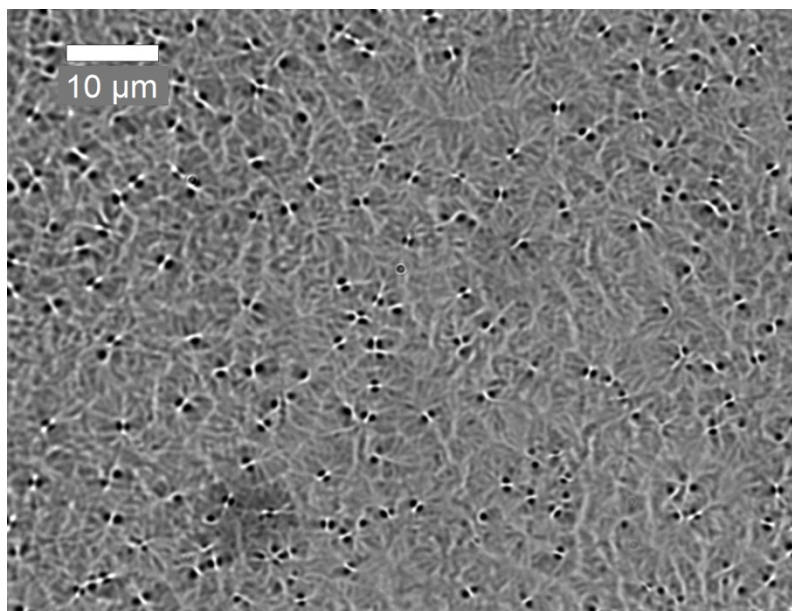


Fig. 1(b) The morphology of spin coated film annealed at 140°C for 3 hours. The eye structure is observed.

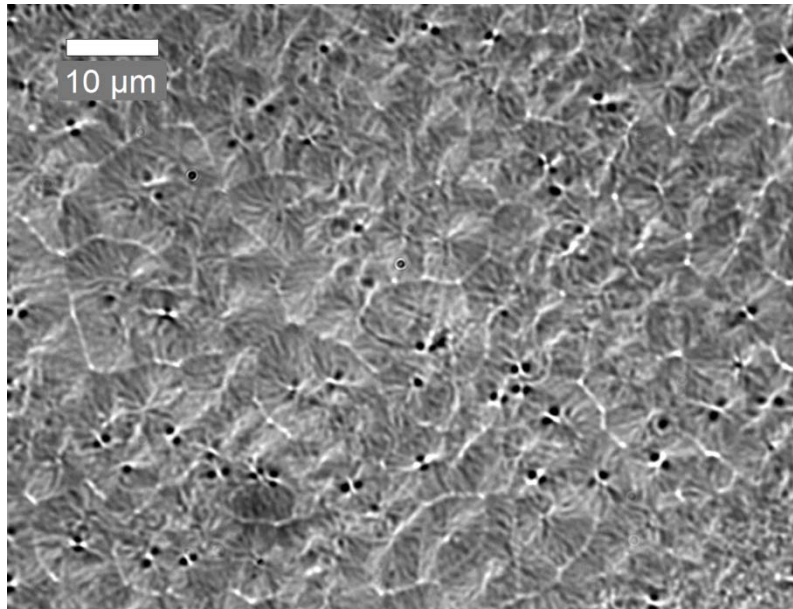


Fig. 2 The morphology of spin coated film annealed at 140°C for 24 hours. Eye structure remains observable while the boundary of spherulites can be more clearly observed. The spherical symmetry does not extend to the center, and the sheaf-like features are preserved.

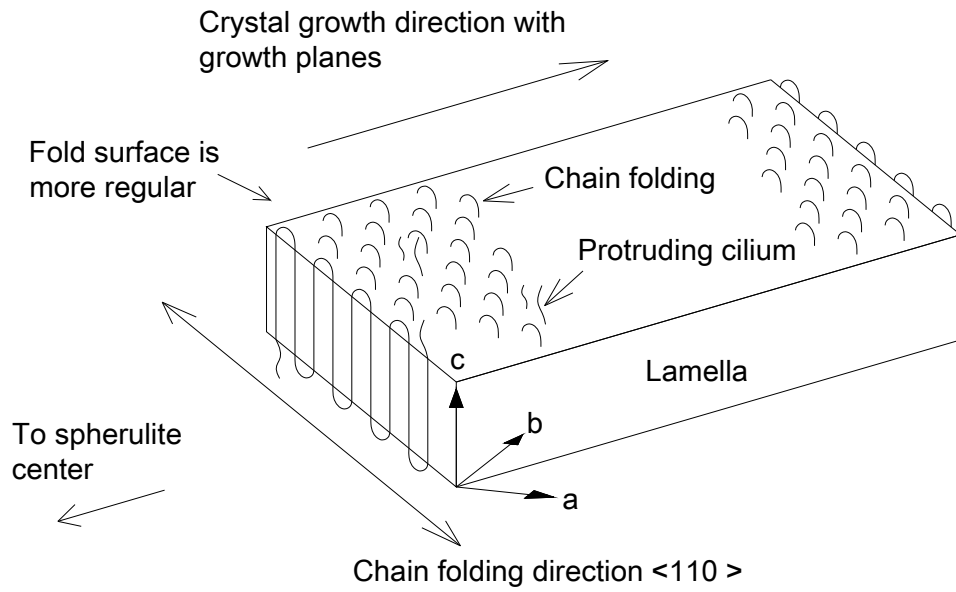


Fig. 3(a) Sketch of the lamellar structure in solvent cast films.

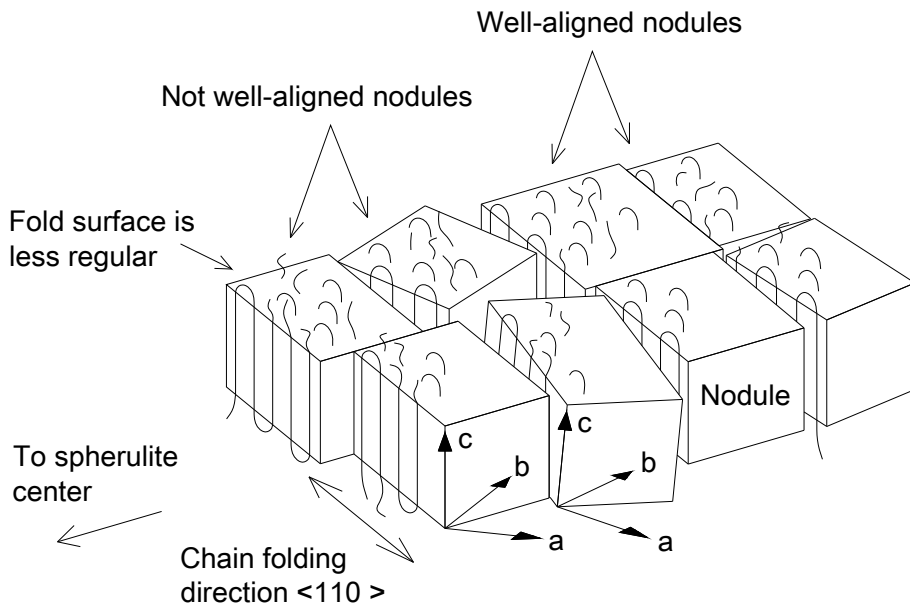


Fig. 3(b) Sketch of the lamellar structure in spin coated films.

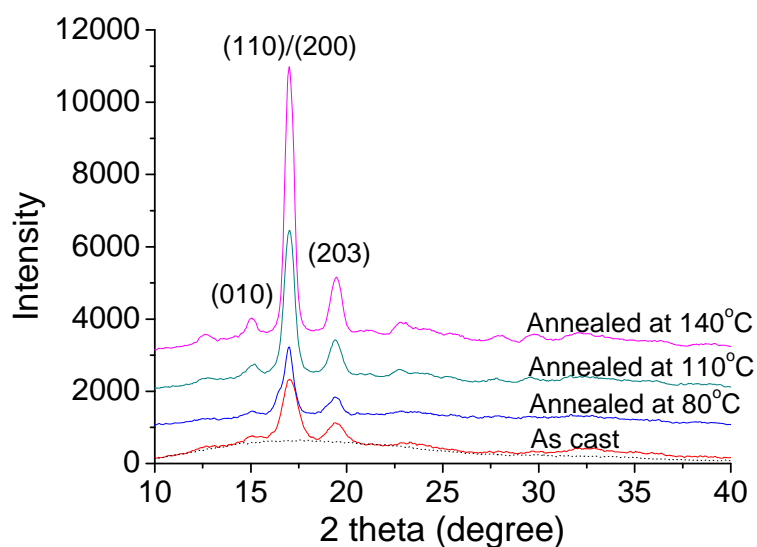


Fig. 4(a) WAXD profiles for solvent cast films annealed at different temperatures for 3 hours. Dotted line under the as cast film is the fitted curve for the amorphous region.

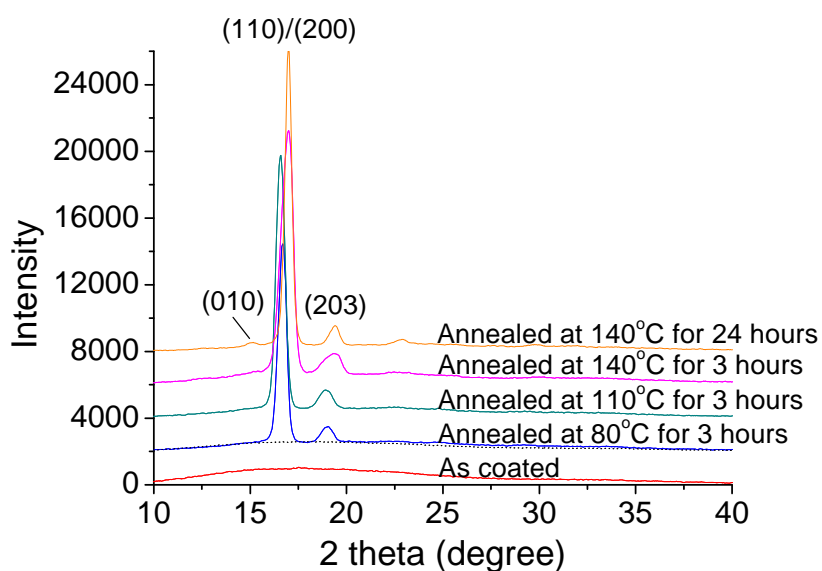


Fig. 4(b) WAXD profiles for spin coated films annealed at different temperatures. The (010) peak start to emerge after 140°C annealing for 24 hours. Dotted line under the 80°C annealed film is the fitted curve for the amorphous region.

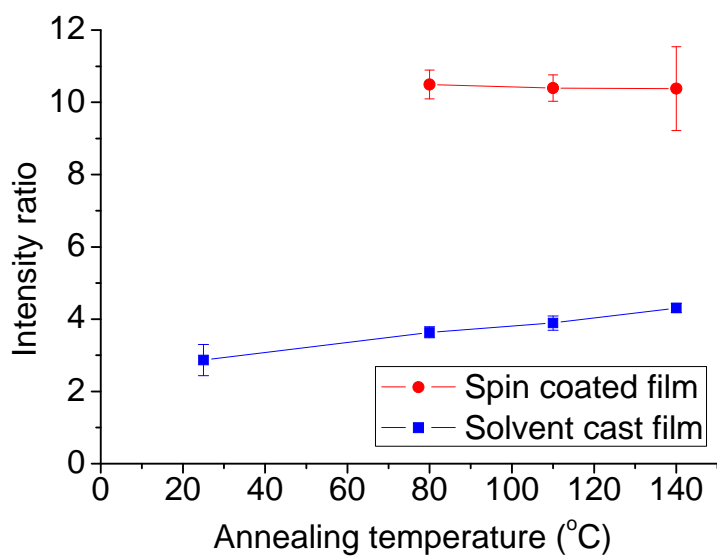


Fig. 5 Intensity ratio  $I_{(110)/(200)}/I_{(203)}$  of the solvent cast and spin coated films annealed for 3 hours. The error bar represents the standard deviation.

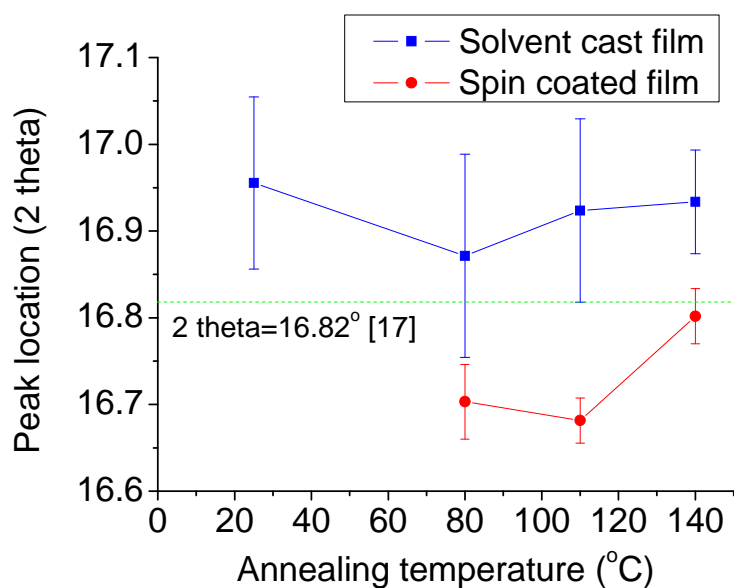


Fig. 6 Location of the (110)/(200) peak for the solvent cast and spin coated films annealed for 3 hours. The error bar represents the standard deviation.

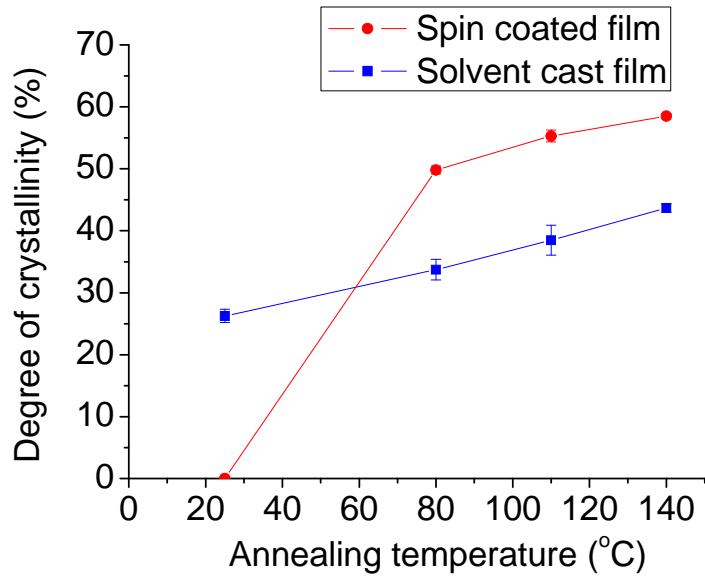


Fig. 7 Degree of crystallinity of the solvent cast and spin coated films annealed for 3 hours. Annealing temperature of 25°C means the as cast film. The error bar represents the standard deviation.

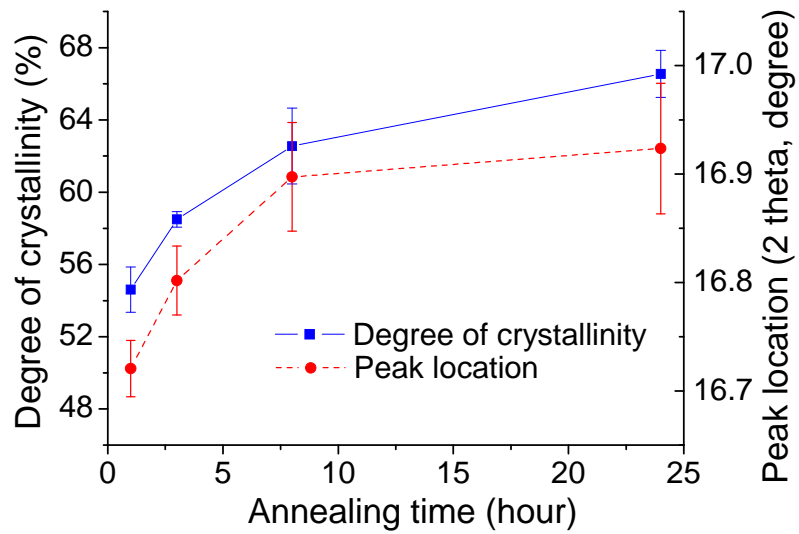


Fig. 8 Degree of crystallinity and peak location of the spin coated films annealed at 140 °C for 1, 3, 8, and 24 hours.

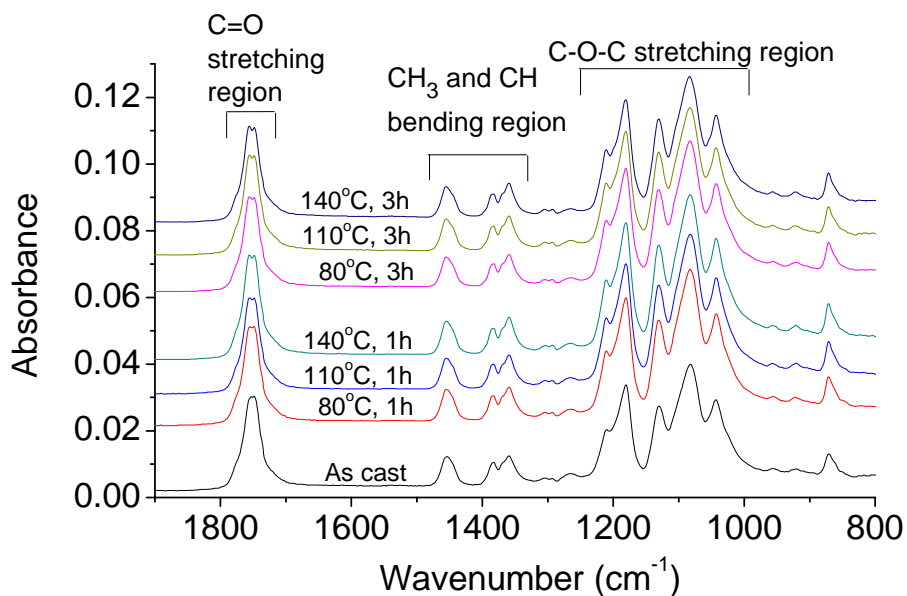


Fig. 9(a) FTIR spectra of the solvent cast films before annealing and after annealed in different conditions.

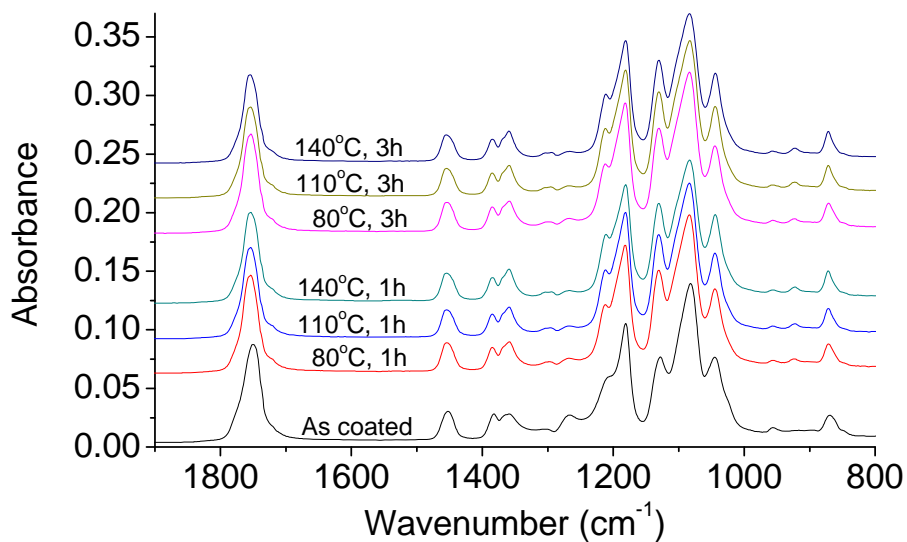


Fig. 9(b) FTIR spectra of the spin coated films before annealing and after annealed in different conditions.

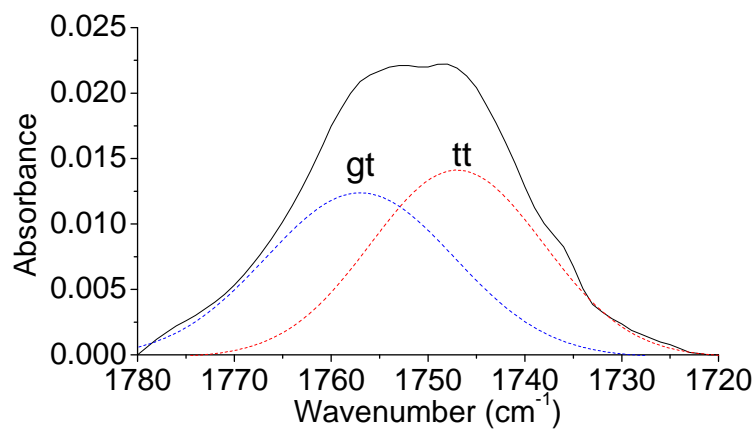


Fig. 10(a) Curve fitting for the *gt* and *tt* conformers in the carbonyl C=O stretching region of the as cast solvent cast film.

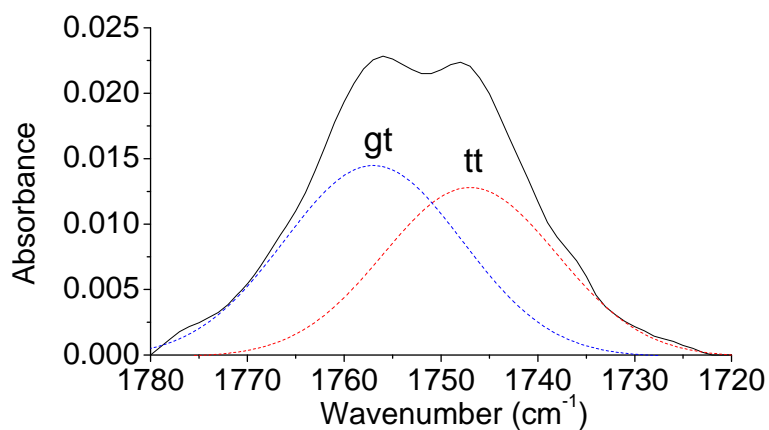


Fig. 10(b) Curve fitting for the *gt* and *tt* conformers in the carbonyl C=O stretching region of the solvent cast film annealed at 140°C for 3 hours.

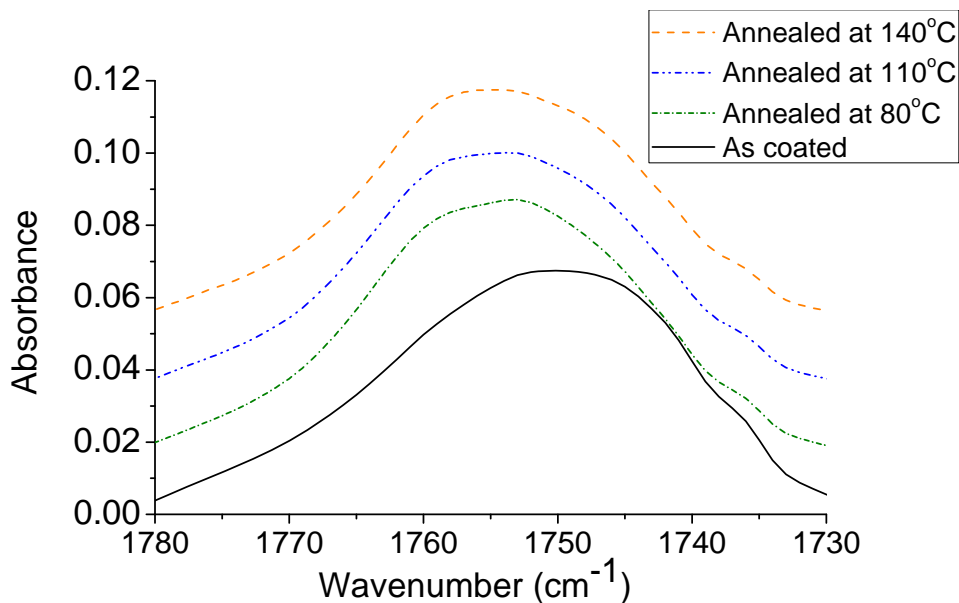


Fig. 11 Carbonyl C=O stretching region of the spin coated films annealed at different temperatures for 3 hours.

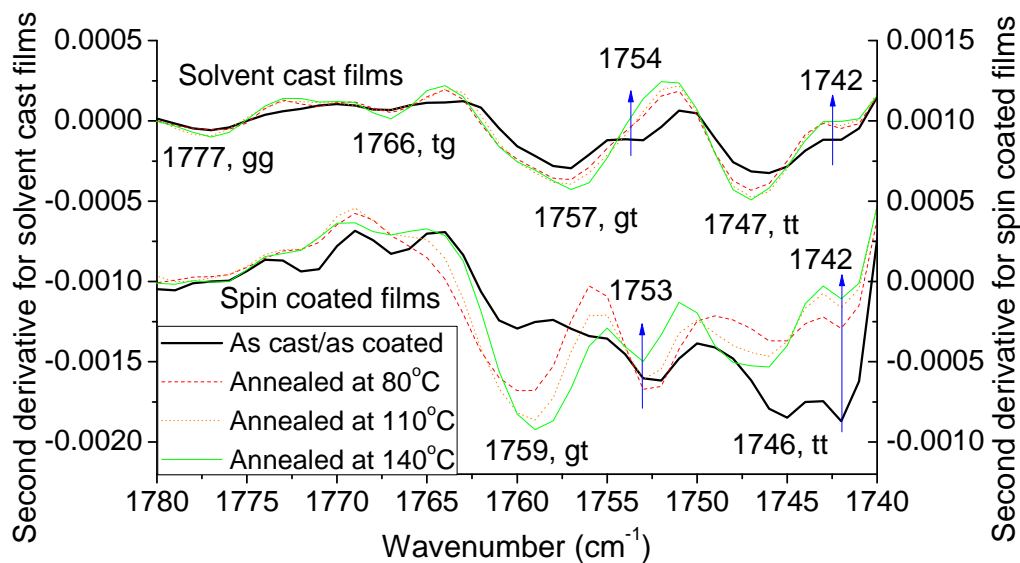


Fig. 12 Second derivative spectra of the C=O stretching region for solvent cast and spin coated films before annealing and annealed at different temperatures for 3 hours.

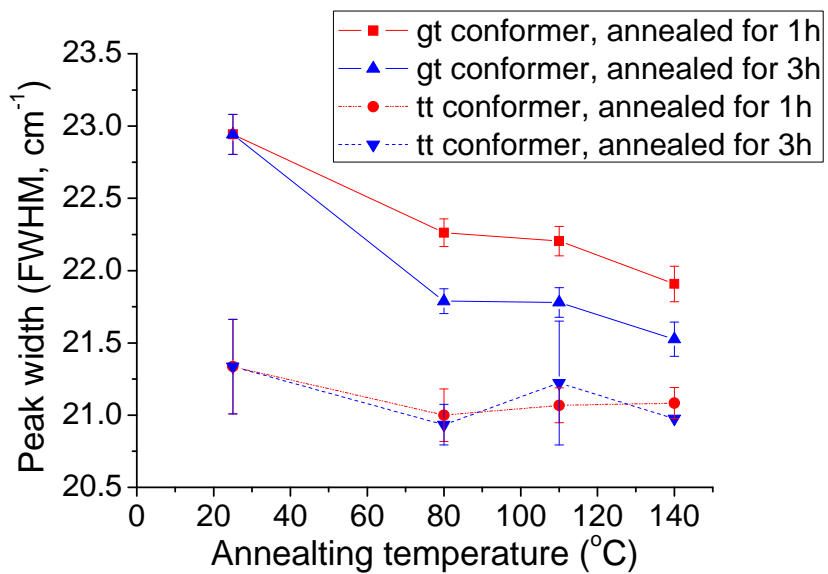


Fig. 13 Peak width of the resolved spectra for the *gt* and *tt* conformers of solvent cast films before annealing and after annealed in different conditions. The error bar represents the standard deviation of the five measurements.